Low Reynolds number airfoil optimization for wind turbine applications using genetic algorithm

Krishnil R. Ram, Sunil Lal, and M. Rafiuddin Ahmed

View Online   Export Citation   CrossMark

ARTICLES YOU MAY BE INTERESTED IN

Experimental study of surface curvature effects on aerodynamic performance of a low Reynolds number airfoil for use in small wind turbines
Journal of Renewable and Sustainable Energy **8**, 053303 (2016); https://doi.org/10.1063/1.4963236

Multi-objective optimization of airfoil shape for efficiency improvement and noise reduction in small wind turbines
Journal of Renewable and Sustainable Energy **6**, 053105 (2014); https://doi.org/10.1063/1.4895528

Turbulent intensity and Reynolds number effects on an airfoil at low Reynolds numbers
Physics of Fluids **26**, 115107 (2014); https://doi.org/10.1063/1.4901969

Low Reynolds number airfoil optimization for wind turbine applications using genetic algorithm

Krishnil R. Ram,[1] Sunil Lal,[2] and M. Rafiuddin Ahmed[1,a]

[1]*Division of Mechanical Engineering, The University of the South Pacific, Suva, Fiji*
[2]*School of Computing, Information and Mathematical Sciences, The University of the South Pacific, Suva, Fiji*

Optimization of a low Reynolds number airfoil for use in small wind turbines is carried out using a Genetic Algorithm (GA) optimization technique. With the aim of creating a roughness insensitive airfoil for the tip region of turbine blades, a multi-objective genetic algorithm code is developed. A review of existing parameterization and optimization methods is presented along with the strategies applied to optimize the airfoil in this study. A composite Bezier curve is used to parameterize the airfoil. The resulting airfoil, the USPT2 has a maximum thickness of 10% and shows insensitivity to roughness at the optimized angles and at other angles of attack as well. The characteristics of USPT2 are studies by comparing it against the popular SG6043 airfoil. While a slight loss in lift is noticed for both airfoils, the drag increments due to early transition are noticeable as well. The airfoil is also studied using computational fluid dynamics (CFD) and wind tunnel experiments during free and forced transition. The USPT2 airfoil will be useful in small wind turbines for locations where blade soiling is likely or where other flow phenomena may cause early transition of the boundary layer. © *2013 AIP Publishing LLC*.
[http://dx.doi.org/10.1063/1.4822037]

I. INTRODUCTION

With rapidly increasing fuel prices and demand for energy, the South Pacific is looking at a possible energy crisis if it does not initiate R&D of renewable energy devices. One of the more mature technologies in renewable energy is wind energy. The South Pacific Islands have a unique challenge in most of the population and spread across the ocean in hundreds of islands. While mega-watt class hydro and wind installations can cater for main islands and population centers, small wind turbines (SWT) are a perfect solution for outer island usage. SWTs range from a few watts to a 100 kW.[1] This scale allows the use of SWTs as village or community power sources and even allows integration into national grids. SWTs can also be mounted on buildings and near homes for personal or mini-grid applications. They are easy to maintain and bring down in times of hurricanes. While the potential for SWTs is being realized worldwide, the SWTs have not yet become as cost effective as their megawatt class counterparts. The European Wind Energy Association (EWEA) has pointed out that there are a number of components of SWTs that need to be improved in order to reduce its cost per kW and make this technology more economical. A major issue reported by EWEA is the need for improved airfoil shapes; variable chord distribution, and variable twist distribution such that the performance of the SWT can be improved significantly.[1] As the airfoil is at the forefront of energy extraction from the wind, the importance of designing efficient and structurally sound blade sections cannot be overemphasized. Since small wind turbines have a smaller chord and operate at lower speeds, these turbines can be classed as operating at low Reynolds numbers. Even though there is no fixed Reynolds number range that bounds the low Reynolds regime, the term

---

a)E-mail: ahmed_r@usp.ac.fj

low Reynolds number has also come to mean the flow regime where the chord Reynolds number is below approximately 500 000.[2] The main focus in the design of blade sections has been to maximize the lift to drag ratio (L/D) mainly by increasing the lift coefficient (C_l).[3] The commonly used NACA airfoils are not appropriate for wind turbines that need to operate in regions of low wind.[4] NACA airfoils are suitable mainly for high Reynolds numbers and relatively small angles of attack (α).[5] Wind turbine airfoils need to perform well over a wide range of angles of attack. This means that the L/D ratio should not drop abruptly as α changes. While numerous airfoils have been developed for high Reynolds number wind turbines, the development of airfoils for small wind turbines has been minimal. Giguere and Selig[6] presented the SG60XX family of airfoils suitable for small wind turbine applications. Apart from these, only a few airfoils are suited to small wind turbines. This study is aimed at adding new airfoils to the existing small collection of small wind turbine airfoils. Airfoil design can be grouped into two main categories: direct design and inverse design. Direct airfoil design using numerical optimization[7] is common and involves manipulating the curves that define the airfoil to achieve desired characteristics. The inverse design approach,[8] which involves generating airfoils to match velocity distributions, can also employ optimization. With the advances in processing powers of computers, optimization of airfoils allows for creation of new airfoils for specialized applications. Genetic Algorithm (GA)[9] optimization is a proven, robust method which utilizes nature's process of evolution to generate optimum solutions. The objective of this study is to design new airfoils for small wind turbines using genetic algorithm optimization. The new airfoils need to have leading edge roughness insensitivity and operate efficiently over a range of angles of attack. A brief review of soiling effects, parameterization methods, and optimization algorithms is presented before the current study is discussed.

A. Soiling effects on wind turbine blades

For optimum performance, the designer needs to look at what happens to a wind turbine in service conditions. The environment a wind turbine operates in plays a major part in determining the performance of the turbine. Several factors such as gusts, turbulence, shadow effects, blade bending moment, noise, and soiling affect a turbine during operation. This paper focuses on designing wind turbine blade sections that are least affected by soiling effects. Soiling is the collection of dust or dirt, mainly across the leading edge of the blade's upper and or lower surfaces. Leading edge roughness due to soiling has many adverse effects. The stall regulation phenomenon in wind turbines is significantly affected by soiling.[10] Ahmed[3] states that when the blade section gathers dust, dirt, etc., it causes early transition of the boundary layer and leads to increased drag. Rooji and Timmer[11] estimated that in large wind turbines, severe nose contamination leads to a loss in power coefficient of each blade segment by 4% and results in loss of 8% for a rotor having a tip speed ratio (TSR) of 8. Corten[12] reports that leading edge soiling can cause multiple stall levels of the rotor and result in production losses of up to 25%.[13] For stall regulated turbines whose angle of attack (α) increases with wind speed, the annual energy loss can be 20% to 30% due to leading edge contamination.[14]

The extent to which roughness affects an airfoil performance is dependent on the nature of the roughness, its size relative to the boundary layer thickness, the Reynolds number and the airfoil type.[15] Numerous researchers have added valuable information to the ongoing research on the effects of leading edge roughness. Freudenreich *et al.*[16] studied the effect of Reynolds number on airfoil roughness using numerical and experimental techniques. Kerho and Bragg[17] investigated the development of the boundary layer and transition due to large leading edge roughness. Zhang *et al.*[18] looked at the effects of roughness at low Reynolds numbers. They carried out particle image velocimetry (PIV) measurements on airfoils with leading edge roughness to observe the flow on the upper surface. They found that in the low Reynolds number case, the maximum lift (rough airfoils) dropped as Reynolds number increased and while small roughness delayed the stall angle, large roughness advanced the aerodynamic stall. The effects of leading edge contamination cannot be ignored during design of airfoils for wind turbines. It is almost certain that leading edge contamination will take place on the turbine blades after

some time and will lead to deterioration in performance if the airfoil geometry is sensitive to roughness effects. In small wind turbines, the tip to mid span region of the blade encounters higher velocities and may encounter dust accumulation along with insects being caught on the dust layers. Low Reynolds number airfoils are particularly sensitive to changes in boundary layer due to leading edge roughness.

This study aims to use a multi-objective genetic algorithm optimization method to generate an airfoil that is insensitive to roughness for α of 4° and 10° . Moderate soiling at 0.08c of the upper surface is introduced in this study. The roughness is simply modeled using a fixed transition point at the desired location. Sections II–V detail the method of airfoil optimization and the results of this study.

II. OBJECTIVE FUNCTIONS

The objective of the algorithm is to maximize the lift while minimizing or fixing the drag in a state of forced transition at 8% of the chord on the upper surface. After many experiments with the optimization algorithms, it was found that improving the performance at multiple angles such as from 4° to 10° is computationally expensive. However, optimizing at the minimum and maximum angles also had the effect of causing nearby angles to be optimized as the lift and drag curves follow a smooth function. For this reason, the airfoil was optimized at angles of 4° and 10°. The objective function was built as follows:

Minimize drag coefficient (C_d), Maximize lift coefficient (C_l) for $\alpha_i .... \alpha_n$

This gives the following generalized fitness function:

$$F(B(u), \mathrm{Re}) = \sum_{i=1}^{n} \left(\frac{Cl_i}{Cd_i * 1.1} \right) \times \frac{1}{m},$$ (1)

where m is the number of angles which is 2 for this case. For this case $\alpha_1 = 4°$ and $\alpha_2 = 10°$. The Reynolds number (Re) chosen for optimization was 200 000 as this is common for small wind turbines to experience. XFOIL's calculation of drag coefficient is normally 9% to 10% lower than experimental values.[19,20] Hence to account for this, the values of drag coefficient from XFOIL are multiplied by a factor 1.1 as shown in Eq. (1). The Bezier curve function is discussed in detail in later sections. To get a much better idea of only leading edge transition effects on the optimization method, the free-stream turbulence intensity was set to a low value of 0.161%.

III. AIRFOIL PARAMETERIZATION AND OPTIMIZATION PROCEDURE

Before optimization can be applied to a problem, it needs to be defined as a mathematical model taking into account all the variables and parameters. In order to optimize the airfoil, the 2D shape of the airfoil needs to be parameterized by defining the variables that will control the coordinates and shape of the airfoil. In this study, the need was for a single discipline shape parameterization scheme whereby only the shape function will be parameterized. It was essential to carry out a study of existing parameterization methods. Samareh[21] provides a detailed review of multidisciplinary parameterization for airfoils. The choice of parameterization depends on the needs of the design problem. The simplest representation of an airfoil is to simply define a sufficient number of x coordinates and the corresponding y coordinates. A large number of (x,y) points are required to approximate the curvature of the airfoil. The discrete y coordinates are joined together as a continuous curve to form the airfoil. In this manner, a very flexible parameterization is obtained; however, great care must be taken to preserve the smoothness and reasonable shape of the airfoil.[22] This method also creates a large number of control variables which would prove computationally expensive to optimize.

Sobieczky[23] proposed a method with ideally low number of control points called the PARSEC parameterization scheme. The PARSEC scheme utilizes the 11 geometric characteristics of the airfoil as control parameters. These control parameters are the leading edge radius,

upper crest position and curvature, lower crest position and curvature, trailing edge direction, trailing edge wedge thickness, trailing edge wedge angle, and trailing edge offset. By controlling these variables, the upper and lower surfaces of the airfoil are generated. The PARSEC method generates realistic airfoil shapes which are easily interpreted by flow solvers and allow for easy convergence. While the PARSEC method is specifically created for airfoil shape generation, it limits the possibility of airfoil shapes especially at the leading edge as mentioned by Castongua and Nadarajah.[24] Also, this method may lead to overlapping of the upper and lower surface, i.e., it does not guarantee a physically acceptable trailing edge.[25]

Recently, Derksen and Rogalsky[26] proposed the PARSEC–Bezier parameterization scheme. This method has been developed to reduce the non-linear interaction of the parameters and create a more direct link of the parameters to the objective function. Airfoil parameterization using B-Splines (Basis splines) is also common as demonstrated by Dhal and Fuglsang[7] and Zhang et al.[27] Similar to Bezier curves, B-splines are constructed using a parameter u and control points. Originally inspired by thin wooden "splines" used in ship design, B-Splines can be considered as a series of Bezier curves connected in such a way that continuity is maintained throughout the curve. B-splines require the calculation of basis functions through recurrence. The de Boor algorithm is normally used to evaluate B-splines.

One of the most common and easiest ways to represent free form curves is via Bezier curves. Bezier curves were originally developed by Paul de Faget de Casteljau as cited by Bieri and Prautzsch[28] and later popularized by Pierre Bezier. Bezier curve parameterization allows the use of a parameter u, and multiple control points P_i to generate x and y coordinates of an airfoil. This study makes use of Bezier curves to parameterize the airfoil. Several studies[8,20,29] have used Bezier airfoil parameterization for airfoil optimization. The Bezier parameterization scheme is easy to implement along with constraints and has reasonable accuracy. The order of the Bezier curve is determined by the number of control points. For $n+1$ control points Pi, a Bezier curve of the nth order will be formed. By joining the control points together, a control polygon is formed. The generalized form of a Bezier curve is defined as

$$\boldsymbol{B}(u) = \sum_{i=0}^{n} \boldsymbol{P}_i \frac{n!}{i!(n-i)!} u^i (1-u)^{n-i}, \quad u \in (0,1),$$ (2)

where $\boldsymbol{B}(u)$ vector contains the x and y coordinates on the curve and $\boldsymbol{P}_i$ contains the x, y coordinates of the control polygon. The parameter u is defined from 0 to 1 uniformly in this study. For this study, a composite Bezier curve was used to define the geometry of the airfoil. One Bezier curve was used to represent the upper surface while a second Bezier curve was used to represent the lower surface as shown in Figure 1.

The start and end control points, $P0$ and $P7$ lie on the airfoil curve itself at the leading and trailing edges and their positions are fixed to maintain a chord length of unity for easier computation and comparison in the flow solver XFOIL. Specific conditions were defined to control the integrity of the airfoil shape at the leading and trailing edge. At the leading edge, the initial
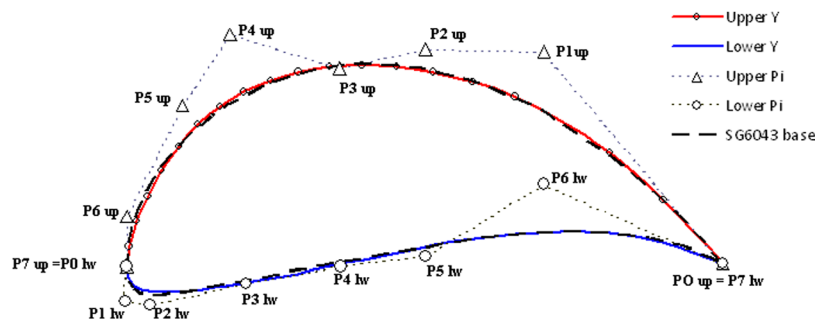

FIG. 1. Bezier curve parameterization of SG6043(6) airfoil using composite Bezier curves, up = upper surface, lw = lower surface. Points P were achieved by interpolation.

and terminal points of the upper and lower curves coincide to close the curve. C^0 continuity is enforced at the trailing edge by simply connecting the upper and lower curve points without any special condition. At the leading edge, C1 continuity was enforced by ensuring that *P1 lw* is a reflection of *P6 up* with the mirror line being perpendicular to segment *P1 lw–P6 up* and crossing at *P7 up*. Despite the leading and trailing edges being fixed, the upper and lower surfaces of the airfoil had a large degree of freedom and had the possibility to represent a suitably large number of free form closed shapes. With the leading and trailing points restricted and *P1 lw* being governed by the coordinates of *P6 up*, a total of 11 control points were available to manipulate the airfoil shape. Higher order (10th) curves were also experimented on but these had increased number of control points and were prone to form bumps due to enhanced local control which was not taken well by the geometry sensitive solver. The 7th order Bezier airfoil parameterization function was coded in C++. Geometric constraints on the airfoil ensured that only realistic airfoil shapes were analyzed. The constraints are described later in the paper.

A. Optimization scheme

The problem of increasing lift and other favorable characteristics of an airfoil while minimizing or maintaining drag and other unwanted traits calls for a suitable multi-objective optimization scheme. In this case the L/D needs to be improved within a given thickness value and causing forced transition on the upper surface of the airfoil. Airfoil shape optimization gives a rapid indication of the possible directions for improvement when direct or inverse geometric cut-and-try is impractical.[30]

Gradient-based optimization models have been used[31,32] for optimization in aerodynamics. This method requires the gradient of the objective function with respect to the shape parameter.[32] The use of neural network models to solve airfoil shape optimization problems has been explored by Huang *et al.*[33] and Khurana *et al.*[34] The Artificial Neural Network (ANN) technique imitates the functioning of the human brain by using artificial neuron connections to recognize complex patterns between input and output data. The use of particle swarm optimization (PSO) in airfoil optimization has been demonstrated by Carrese *et al.*[35] The PSO mimics the characteristics of a flock of birds to gain optimal solutions. The term particle refers to candidate solutions in the PSO algorithm. Particles identify and exploit promising areas of the design space by learning from previous experience and emulating the success of other particles.

Evolutionary algorithms (EA) are by far the most popular in airfoil optimization. Evolutionary algorithms are based on the neo-Darwinism paradigm of evolution. Two common variants of EA in airfoil optimization are Differential Evolution (DE) and Genetic Algorithm Optimization. Differential evolution was originally developed by Price[36] and is mostly used for real valued functions. This meta-heuristic optimization approach works on generating candidate solution vectors and improving on them through re-combination with other solution vectors from the population.

The GA optimization approach was developed by Holland[9] and has seen use in numerous optimization problems owing to its robust approach. The GA optimization has been used by Grasso[29] and others[8,19,37–39] for airfoil development. The GA is a stochastic algorithm and it keeps in memory a population of solutions during iteration rather than a single solution.[40] GA uses a direct analogy of natural behavior. But before GA can be run, a suitable coding (or representation) for the problem must be devised.[41] While conventional GA represented the population of solutions in binary bits, recent developments have allowed for real valued GA approach. The solutions of GA are coded as an array of bits called chromosomes or genotype. The genotype represents an individual in a solution vector called the phenotype.

GA is an iterative process and each iteration is called a generation. The initial population is made up of individual solutions represented in chromosomes. Each individual is subjected to a fitness function that will determine its fitness values. Normally the chromosomes with the desired or closer to desired fitness values are chosen to be parents in the next generation. During selection it is common to use a roulette wheel. Here, the selection is made biased by assigning better solution a higher probability of getting selected. The parents are then mated

using crossover methods to form the next population set. A crossover ratio (C_r) is a parameter which expresses the probability that a selected pair of parent chromosome will crossover to produce the next generation of offspring's. Likewise, the mutation ratio (M_r) is the probability that a given chromosome will develop random mutation in the next population. Mutation is an evolutionary mechanism to add diversity in the population, and it helps to a certain extent in escaping premature convergence to a local optima. The fitness function is repeated on the next set of population until a termination condition is reached. The termination condition may be reached if a satisfactory solution is found or at the end of the generations. This study utilizes the binary coded GA written in C++ by Lal *et al.*[42] Figure 2 shows the flow of information in the GA optimization. Initialization of the population also includes seeding of the popular SG6043 airfoil control points. Since GA optimizes the control points of the Bezier functions that governed the airfoil shapes, the 11 control points were discretized into a bit string of 88 bits with each control point represented using 8 bits.

B. Setting geometric constraints and fitness evaluation

The flow solver used in this study is highly sensitive to geometry and hence strict geometry conditions are set to prevent unnecessary analysis and failure of analysis by passing nonrealistic airfoil shapes to the solver.

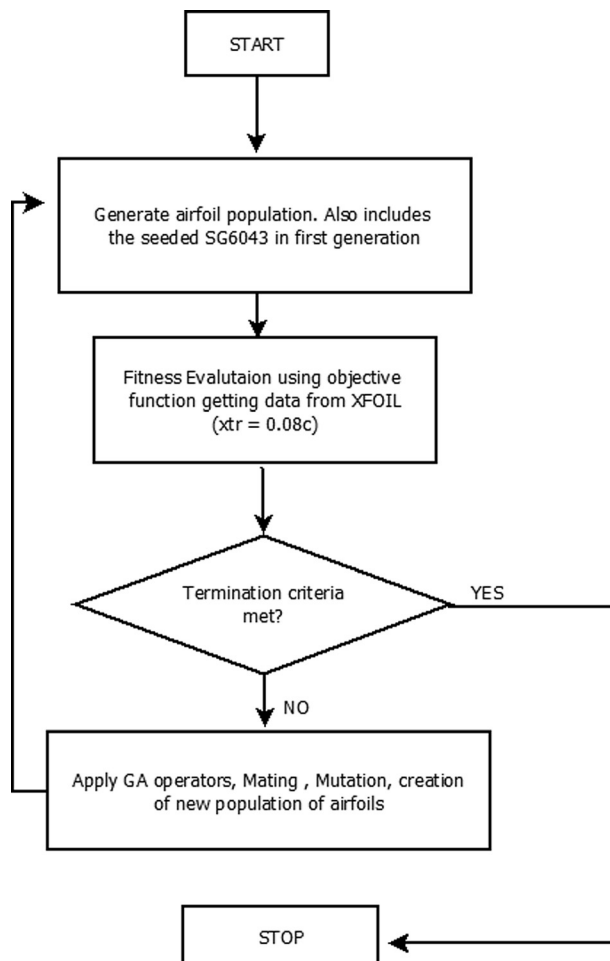To ensure that the upper and lower Bezier curves do not overlap, the following condition was set:

FIG. 2. Flowchart for airfoil optimization using GA.

$$Y(u)_{upper} - Y(u)_{lower} > 0, \quad (\text{Except for } P0 \text{ and } P7). \tag{3}$$

To maintain structural strength of the wind turbine blade, the blade section must be sufficiently thick. The thickness is maintained between 8% and 14% of the chord using the following condition:

$$0.14c > \left(Y(u)_{upper} - Y(u)_{lower}\right) > 0.08c. \tag{4}$$

The upper and lower limits of the y coordinates were set to prevent very highly cambered airfoils and to maintain a realistic search space. The x coordinates were fixed in order to reduce the number of control variables,

$$\left(Y(u)_{upper}\right) \leq 0.2 \quad \left(Y(u)_{lower}\right) \geq -0.1. \tag{5}$$

Instead of coding the constraints along with the individual solutions, the solutions are allowed to violate these conditions initially. Once the shapes are created, a pre-fitness evaluation is done and the shapes that are not conforming to any of the geometric conditions are assigned the lowest fitness value of 1 and further analysis of these curves is not permitted. The popular panel method viscous-inviscid flow solver XFOIL[43] was used to calculate the C_l and C_d values of the airfoils at pre-defined Reynolds numbers and α. The C_l and C_d values were input to the fitness function (Eq. (1)). The resulting airfoil presented herein was obtained after performing numerous runs which terminated at 3000 generations. The average and best fitness value for part of the iteration is shown in Figure 3. The GA parameters were empirically tuned as follows: $C_r = 0.65$, $M_r = 0.15$, and population size of 101.

IV. EXPERIMENTAL AND COMPUTATIONAL FLUID DYNAMICS (CFD) ANALYSIS

Numerical analysis was performed on the USPT2 airfoil using ANSYS ICEM-CFD and CFX software. Flow over the airfoils was analyzed for different α and Re values. A hexahedral mesh based on O-grid and C-grid topologies was created around the foil with 300 000 nodes. The mesh density was increased near the leading and trailing edge to capture the peak suction, stagnation, and transition points. A k-ω shear stress and transport turbulence model was used. The study focuses on moderate amount of soiling that will cause transition but not separation; hence, the trip-wire (Figure 4) was made sufficiently small to ensure that it did not cause separation. The airfoil was also tested in XFOIL from $0°$ to $18°$. Essential characteristics such as C_l and C_d were noted and compared with experimental results. An open circuit, suction type low speed wind tunnel was used. The Engineering Laboratory Design (ELD) Inc wind tunnel in
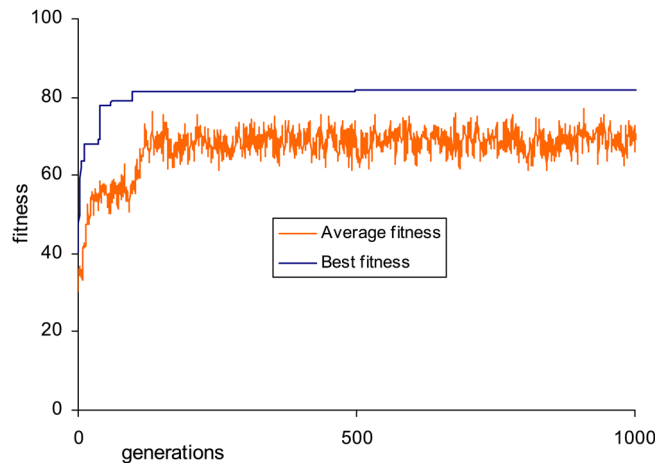

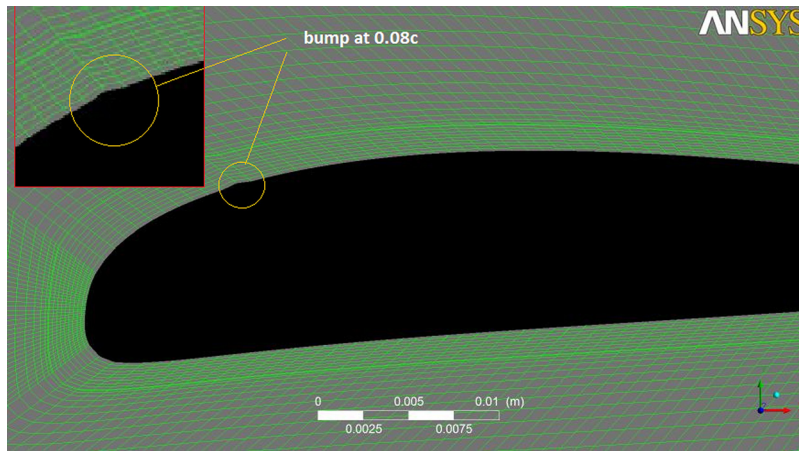FIG. 3. Fitness value changes over several generations.

FIG. 4. A noticeable yet small trip-wire is added to the airfoil at 0.08% of the chord to simulate soiling and cause transition of the boundary layer.

the Fluids laboratory at the University of the South Pacific that can give a velocity range of 3 m/s to 48.77 m/s in the test section was used. A centrifugal fan powered by a 10 HP, AC 3-phase thyristor-controlled motor is used to generate the airflow. A maximum velocity resolution of 0.08 m/s is achievable in the test section. The test section measures 305 mm × 303 mm × 1000 mm. A traversing pitot-static tube was used to measure the velocity in the wind tunnel test section. Furness Controls FCO510 digital micro-manometer was used to take pressure readings. The USPT2 profile was milled out of wood and 23 pressure taps (0.8 mm diameter) were provided on the upper surface and 13 on the lower surface. The test model airfoil has a span to chord ratio of 3.03 (Chord = 100 mm) for pressure measurements. The test profile of USPT2 was polished to ensure a smooth surface. A separate section of the airfoil was milled and finished without any pressure taps and a span to chord ratio of 4.04 (chord = 75 mm). This was for direct lift (L) and drag (D) force measurements. A two component lift and drag dynamometer equipped with a Linear Variable Differential Transformer (LVDT) was used. The dynamometer has an accuracy of 1 g(f) which is equivalent to 0.01N. The accuracy of lift and drag coefficients also depends on the measurements of airfoil area, air density, and velocity. Uncertainties in all these measurements allow measurement of C_l to an accuracy of 0.01 and C_d to an accuracy of 0.007. A maximum lift force of 84N can be measured while a maximum drag of 45N can be measured by the dynamometer. The airfoil was tested at a Reynolds number of 200 000 and the results were compared with XFOIL results. A trip wire (0.6 mm diameter) was used to force transition at 0.08c experimentally. Solid blockage was applied to correct the velocity in the wind tunnel for lift calculations while the wake blockage correction was applied to drag values. During solid blockage the airfoil volume blocks and redirects flow over it, thus increasing the velocity over the airfoil. The change in velocity is found by multiplying the blockage correction factor by the free stream velocity. The correction factor is given as

$$\varepsilon_{sb} = \frac{K_1 V_{airfoil}}{S^{\frac{3}{2}}},$$ (6)

where $K_1 = 0.74$ if the model spans from wall-to-wall and $K_1 = 0.92$ if there is a small gap between the model and the wall, S is the effective section area and V is the volume of the airfoil. The wake blockage correction is applied to correct the rise in air velocity in the tunnel due to airfoil wake. The wake blockage correction is given by

$$\varepsilon_{wb} = \frac{c}{2h} C_d,$$ (7)

where h is the height of the wind tunnel test section and C_d is the uncorrected drag.

V. RESULTS AND DISCUSSION

Figure 5 shows the resulting airfoil in comparison with the seeded airfoil SG6043. Seeding an airfoil in the optimization code meant that rather than starting with no knowledge of an airfoil, the algorithm is fed an actual low Reynolds number airfoil in the first generation which makes its search easier.

The optimizations were aimed at making the airfoil less sensitive to soiling and to perform better over a wide range of α. USPT2 has a maximum thickness of 10.036% of the chord. The maximum thickness has moved closer to the leading edge. A slight bulge is also noticeable in the belly of the airfoil along with an increment in nose radius.

Twenty two pressure taps were provided on the upper surface and thirteen on the lower surface to measure the pressure distribution on the airfoil. The pressure was non-dimensionalised to give Coefficients of pressure (Cp). Pressure distributions in terms of Cp are useful in determining the flow phenomena over and airfoil. Figure 6 shows the Cp values on the USPT2 airfoil during free transition at 6° and 200 000 Reynolds number. Peak suction values are experimentally lower than those predicted by XFOIL and ANSYS CFX. Transition occurs at around 0.25c at 6° (Figure 6) and this is well predicted by XFOIL which predicts transition at around 24% of the chord. As shown in Figure 6, the pressure distribution on the suction side shows a kink at around 0.25c, which is normally taken as the location of transition. The experimental pressure distribution values are in agreement with the predicted values at most of the locations.
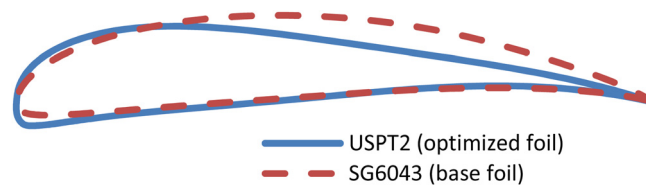

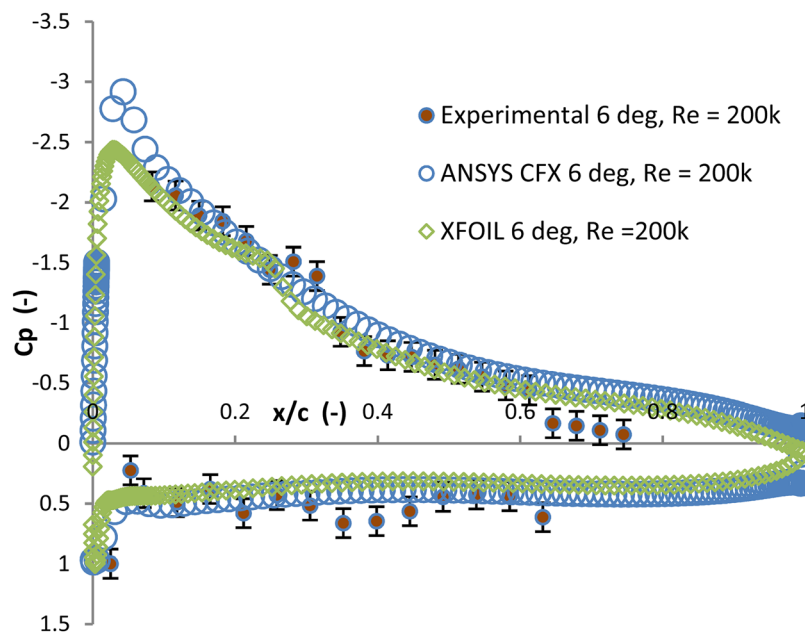FIG. 5. The resulting airfoil USPT2 geometry compared to SG6043 airfoil.

FIG. 6. Coefficients of pressure (Cp) of the USPT2 section at 6° and 200 000 Reynolds number during free transition.

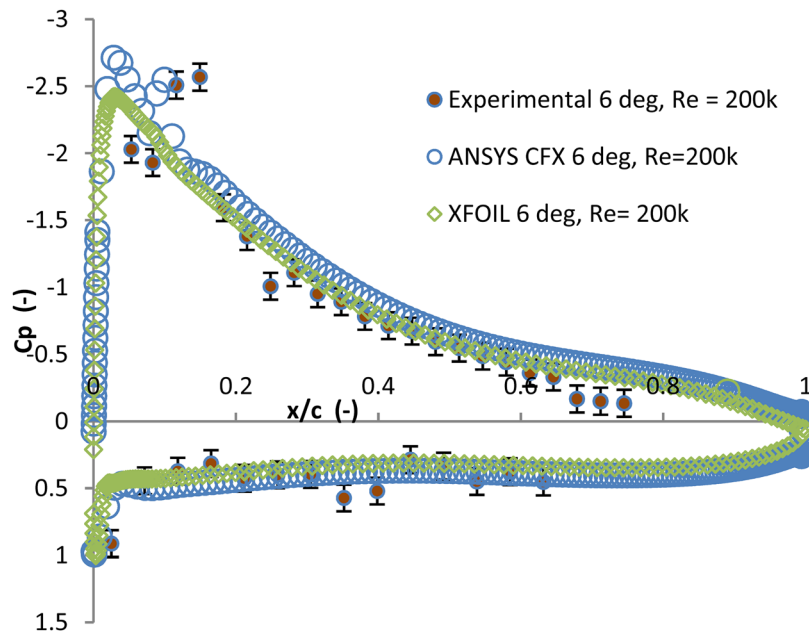FIG. 7. Coefficients of pressure (Cp) of the USPT2 section at 6° and 200 000 Reynolds number while forcing transition at 0.08c.

For the forced transition case, the pressure distribution (Figure 7) shows a second suction peak in ANSYS CFX just after the transition location. This could be caused by the acceleration of flow over the trip-wire which was created at 0.08c along with the fact that the trip-wire causes transition of the boundary layer from laminar to turbulent. The turbulent layer is more energetic. Experimental results show the suction peak just after the transition location in the simulated soiled region. The pressure gradient on the upper surface is favorable with the pressure recovery taking place till the trailing edge.

Lift coefficients are shown in Figure 8 for different α and for both forced and free transition cases. There is very little variation in the lift for USPT2 during clean and rough conditions. Smooth stall occurs at 13° in both cases for USPT2. Between 4° and 10°, the maximum drop in the lift value is around 1.75% (XFOIL) 5% experimentally (Figure 8). For SG6043 a smooth stall also occurs at around 16° in both cases. However, the maximum lift values are lower for

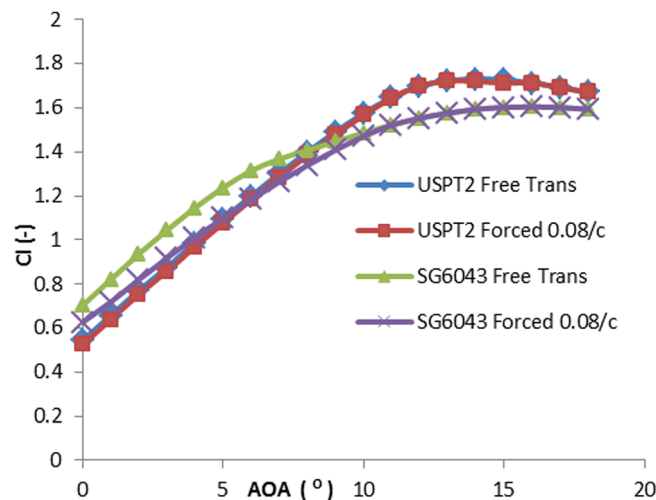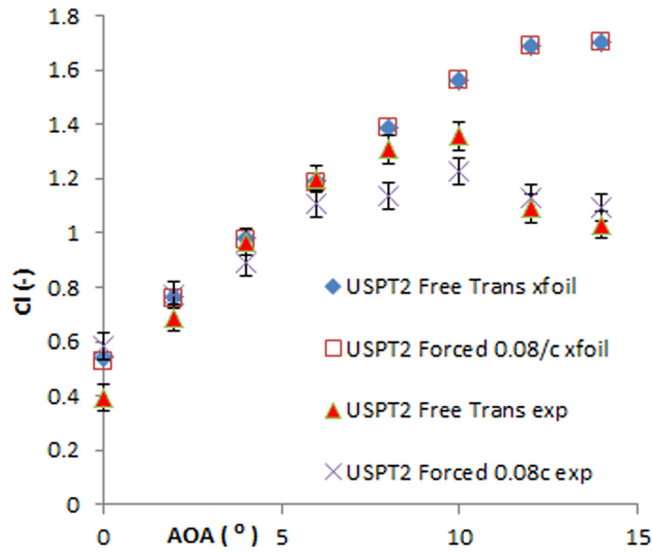FIG. 8. Lift coefficients of the airfoils are compared for free and forced transition at Re = 200 000.

FIG. 9. Experimental and numerical (XFOIL) lift coefficients for USPT2 at Re = 200 000.

SG6043 in both cases compared to the optimized foil. Between 4° and 10°, the maximum drop in lift coefficient is around 11%.

Figure 9 shows the experimental lift coefficients for USPT2 airfoil compared to XFOIL results. The lift values are in agreement apart from the fact that stall is predicted at 10° and not 13°. Post stall lift values are also much lower than that predicted by XFOIL.

The drag values for the USPT2 airfoil are lower from 9° onwards compared to SG6043 as shown in Figure 10. Between angles 4° and 10°, where the optimization was performed, the free transition SG6043 case has the least drag and this explains the higher L/D values. But once transition occurs at the leading edge, the SG6043 airfoil exhibits a rise in drag at angles below 10°. The drag values in the SG6043 airfoil almost double at some angles below 10° and above 4° due to the forced transition. Between 4° and 10° the USPT2 has a maximum 13% rise in drag values once transition is enforced.

The experimental drag values are slightly higher than those predicted by XFOIL; this had already been factored into the objective function. Experimental values at low angles of attack are closer while at higher angles, the experimental drag is slightly higher. This is seen in
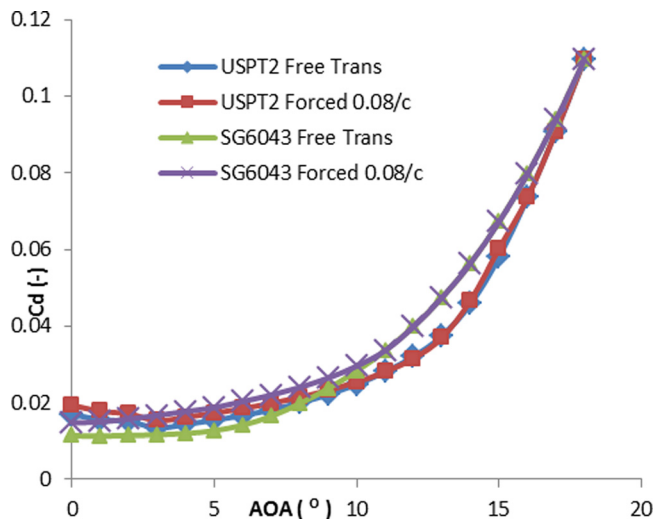

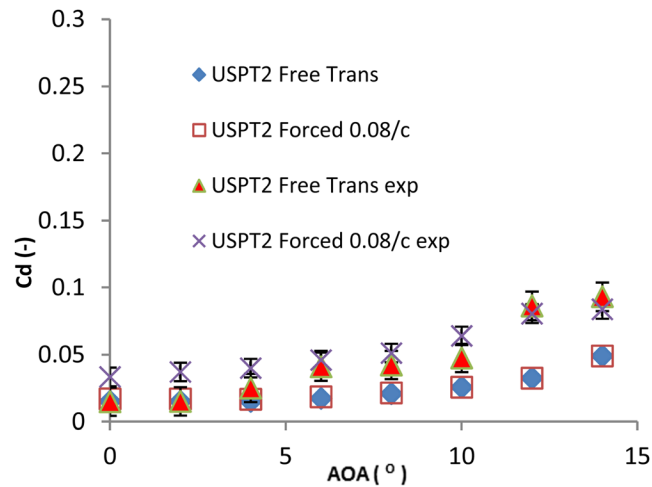FIG. 10. Drag coefficients for the airfoils for forced and free transition cases at Re = 200 000.

FIG. 11. Experimental and numerical (XFOIL) drag coefficients for USPT2 at Re = 200 000.

Figure 11. It must be noted that the XFOIL drag values in Figure 11 were computed at a turbulence intensity of 1.51% which bears closer resemblance to the wind tunnel turbulence. Overall both the forced and free transition airfoils have low drag values till 10° after which drag increases rapidly.

Figure 12 shows the lift to drag ratio of the airfoils for different α. The SG6043 airfoil has greater L/D for free transition, i.e., clean leading edge. Once transition is forced at 0.08c, the performance of the airfoil deteriorates considerably. The forced transition has very little effect on the performance of the USPT2 airfoil. Also interesting to note is that in both the forced and free transition cases, the USPT2 outperforms the SG6043 from 9° to 15°.

The USPT2 not only has better insensitivity to roughness but also performs well at higher α in both clean and dirty conditions. This makes the USPT2 a useful airfoil for tip region of small wind turbines, especially with passive stall regulation. The transition location of the airfoils was also compared in XFOIL for free transition cases and is shown in Figure 13.

For USPT2, the transition point at low angles is naturally located upstream due to the geometry of the airfoil. Once transition takes place the effect on the performance of the airfoil is little, since the shift in transition location from the clean to rough case is small. This is not the case for the SG6043 airfoil which has transition points far downstream; the transition at the leading edge which is the most likely effect of soiling causes a vast difference in transition location and results in poor performance.
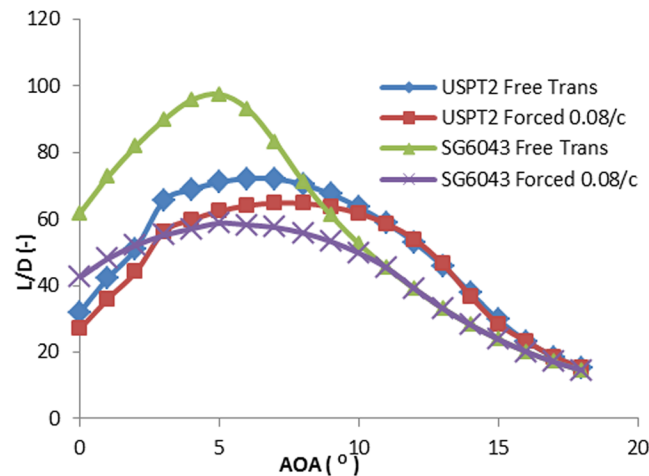

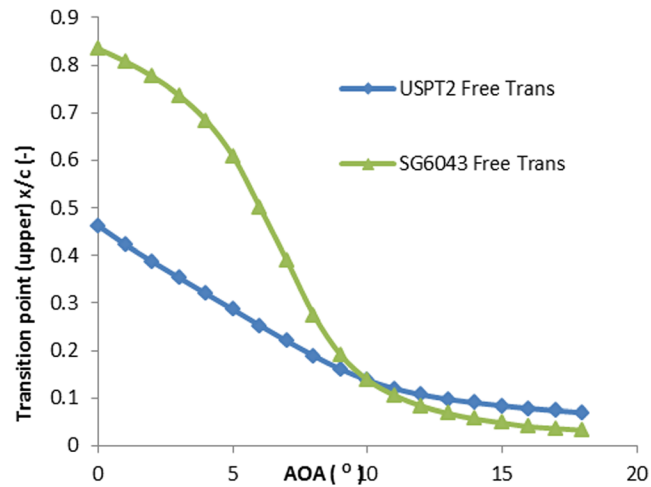FIG. 12. Lift to drag ratio of the airfoils for free and forced transition cases at Re = 200 000.

FIG. 13. Location of transition on the upper surface for the two airfoils for the case of free transition at Re = 200 000.

The skin friction drag which is caused by the viscous effects on the airfoil surface is presented for different angles of attack in Fig. 14. For SG6043 during free transition, the skin friction drag is initially low and rises with α until 10° after which it drops. This is linked to the location of transition on the foil. During free transition, the boundary layer remains laminar for a long time and incurs lower friction drag. Once transition is forced to the leading edge, the friction drag rises significantly (as much as 69% at 4°). In case of the USPT2 during free transition, the skin friction drag is higher at the lower α and drops abruptly before the angle of optimization (4°). The skin friction rises very slowly and starts to drop before 10°. The increased skin friction drag due to the presence of a turbulent boundary layer after transition point may be one of the reasons for the drop in performance of the SG6043. The USPT2 incurs additional skin friction after forced transition but this is small since the difference in transition location for the rough and smooth case is small. The airfoil was analyzed using ANSYS CFX and a small trip-wire was used to simulate transition at 0.08c. Figure 15 shows an increase in turbulent kinetic energy immediately after the trip-wire location signifying transition to turbulent boundary layer. The turbulent boundary layer is more energetic and less susceptible to separation.
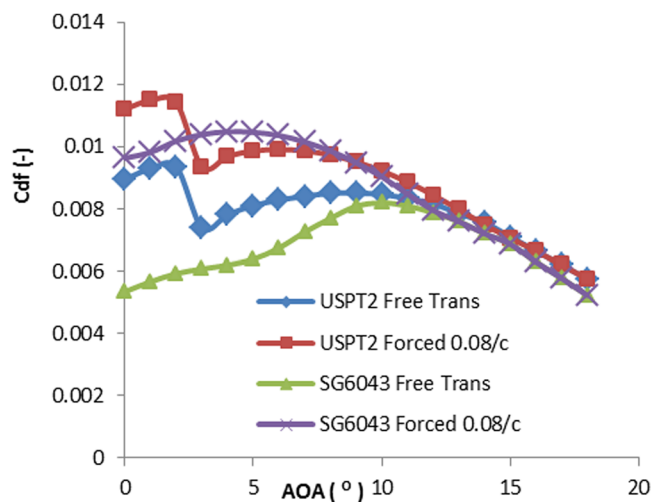

FIG. 14. Skin friction drag for the airfoils at Re = 200 000.
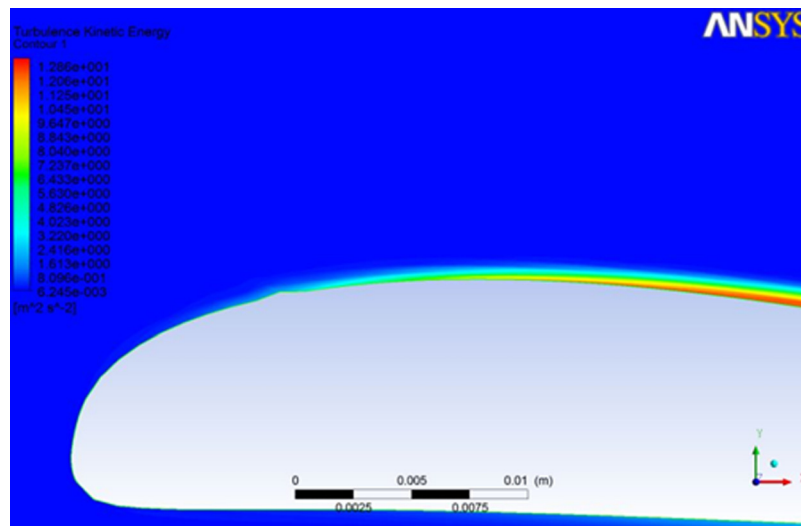
FIG. 15. Increase in the Turbulence Kinetic Energy soon after the trip-wire indicating transition of the laminar boundary layer to turbulent.

VI. CONCLUSIONS

The design and characteristics of a low Reynolds number roughness insensitive airfoil, the USPT2, are presented. Due to soiling, the transition point location moves further upstream and deteriorates the performance of airfoils that usually have laminar boundary layer over majority of the chord. The USPT2 naturally has transition locations close to the leading edge and a shift in the transition point upstream due to soiling does not drastically change its performance. USPT2 has a maximum thickness of 10% which is suitable for the tip to mid span region of small wind turbines. The airfoil has optimized performance between $4°$ and $10°$. During clean and dirty conditions, the new airfoil also has higher L/D than most airfoils such as SG6043 after $10°$. The airfoil is suitable for design angles around $6°$ in fixed pitch small wind turbines. The airfoil stalls at around $13°$ and where it also attains a maximum C_l of 1.72. The maximum L/D ratio of around 72 ($Re = 200\,000$) is attained in clean conditions for the USPT2 and this falls to around 64.7 in soiled conditions due to early transition. Furthermore, the L/D ratio does not drop abruptly at high angles as in other low Reynolds number airfoils. This smooth decline ensures that the turbines performance does not change abruptly at high angles.

[1]EWEA, *Wind Energy—The Facts* (European Wind Energy Association, 2010).
[2]P. Giguère and M. S. Selig, Wind Eng. **27**, 367 (1997).
[3]M. R. Ahmed, Int. J. Energy Res. **36**, 829 (2012).
[4]M. R. Ahmed, S. Narayan, M. A. Zullah, and Y. H. Lee, J. Fluid Sci. Technol. **6**, 357 (2011).
[5]H. Fupeng, L. Yuhong, and C. Zuoyi, Wind Eng. **25**, 105 (2001).
[6]P. Giguère and M. S. Selig, J. Sol. Energy Eng. **120**, 108 (1998).
[7]K. S. Dahl and P. Fuglsang, *Design of the Wind Turbine Airfoil Family Riso-a-Xx*, (National Laboratory Roskilde, Denmark, 1998).
[8]B. A. Gardner and M. S. Selig, "Airfoil design using genetic algorithm and an inverse method," AIAA Paper No. 2003–0043, 2003.
[9]J. H. Holland, *Adaptation in Natural and Artificial Systems: An Introductry Analysis with Applications to Biology, Control and Artificial Intelligence* (University of Michigan Press, Ann Arbor,1975).
[10]N. Ren and J. Ou, J. Electromagn. Anal. Appl. **1**, 102 (2009).
[11]R. P. J. O. M. van Rooji and W. A. Timmer, J. Sol. Energy Eng. **125**, 468 (2003).
[12]G. P. Corten and H. F. Veldkamp, Nature **412**, 42 (2001).
[13]H. A. Madsen, *Aerodynamics of Horizontal Axis Wind Turbine in Natural Conditions* (Riso National Laboratory, Roskilde, 1991).

[14]J. L. Tangler and D. M. Somers, *NREL Airfoil Families for HAWTS* (National Renewable Energy Laboratory, Colarado, 1995).

[15]F. R. Marzabadi, M. R. Soltani, and M. Masdari, in *ICAS 2010: Proceedings of the 27th International Congress of International Council of the Aeronautical Sciences*, Nice, France, 19–24 September 2010, edited by I. Grant (Optimage Ltd on behalf of ICAS, London, 2010) paper ICAS2010-3.2ST2.

[16]K. Freudenreich, K. Kaiser, A. P. Schaffarczyk, H. Winker, and B. Stahl, Wind Eng. **28**, 529 (2004).

[17]M. F. Kerho and M. B. Bragg, AIAA J. **35**, 75(1997).

[18]T. Zhang, T. Igarashi, and H. Hu, "Experimental Investigation on the performance degradation of low reynolds number airfoil with distributed leading edge roughness," AIAA Paper No. 2011–1102, 2011.

[19]W. A. Timer, "An overview of NACA 6-digit airfoil series characteristics with reference to airfoils for large wind turbine blades," AIAA Paper No. 2009–268, 2009.

[20]N. Bizzarrini, F. Grasso, and D. P. Coiro, "Numerical optimization for high efficiency, low noise airfoils," AIAA Paper No. 2011–3187, 2011.

[21]J. A. Samareh, in *CEA/AIAA/ICASE/NASA Langley International Forum on Aeroelasticity and Structural Dynamics: Proceedings CEA/AIAA/ICASE/NASA Langley International Forum on Aeroelasticity and Structural Dynamics*, Williamsburg, America, 22–25 June 1999; NASA/CP: 1999–209136/PT1, pp. 333–343.

[22]J. Hájek, in *WDS Proceedings of the 16th Annual Conference of Doctoral Students*, Prague, Czech Republic, 5–9th June (Matfypress, Prague, 2007), pp. 233–240.

[23]H. Sobieczky, Notes Numeri. Fluid Mech. **65**, 71 (1999).

[24]P. Castongua and S. K. Nadarajah, "Effect of shape parameterization on aerodynamic shape optimization," AIAA Paper No. 2007–59, 2007.

[25]A. Shahrokhi and A. Jahangirian, Aerosp. Sci. Technol. **11**, 443 (2007).

[26]R. W. Derksen and T. Rogalsky, Adv. Eng. Softw. **41**, 923 (2010).

[27]F. Zhang, S. Chen, and M. Khalid, in *ICAS 2002, Proceedings of the 23rd Congress of International Council of the Aeronautical Sciences 2002*, Toronto, Canada, 8–13 September 2002, edited by I. Grant (Optimage Ltd on behalf of ICAS, London, 2002), Paper ICAS2002–2.11.1.

[28]H. P. Bieri and H. Prautzsch, Comput. Aided Geom. Des. **16**, 579 (1999).

[29]F. Grasso, "Usage of numerical optimization in wind turbine airfoil design," AIAA Paper No. 2010–4404, 2010.

[30]M. Drela, "Frontiers of Computational Fluid Dynamics," in *World Scientific Pros and Cons of Airfoil Optimization*, edited by D. A. Caughey and M. M. Hafez (World Scientific, Singapore,1998), pp. 363–380.

[31]A. March, K. Willcoxy, and Q. Wangz, Aeronaut. J. **115**, 729 (2011).

[32]S. B. Hazra, "An efficient method for aerodynamic shape optimization," AIAA Paper No. 2004–4628, 2004.

[33]S. Y. Huang, L. S. Miller, and J. E. Steck, "An exploratory application of neural networks to airfoil design," AIAA Paper No. 94–0501, 1994.

[34]M. S. Khurana, H. Winarto, and A. K. Sinha, "Application of swarm approach and artificial neuralnetworks for airfoil shape optimization," AIAA Paper No. 2008–295, 2008.

[35]R. Carrese, H. Winarto, and J. Watmuff, in *ICAS 2010: Proceedings of the 27th International Congress of International Council of the Aeronautical Sciences*, Nice, France, 19–24 September 2010, edited by I. Grant (Optimage Ltd on behalf of ICAS, London, 2010), Paper ICAS 2010–2-6.4.

[36]K. V. Price, in *Biennial Conference of the North American Fuzzy Information Society 1996*; Proceedings of Fuzzy Information Processing Society, 1996. NAFIPS,. 1996 Biennial Conference of North America,Vacaville, USA, 19–22 June (IEEE, New York, 1996), pp. 524–527.

[37]D. Quagliarella and A. Vicini, Finite Elem. Anal. Des. **37**, 365 (2001).

[38]I. De Falco, R. D. Balio, A. D. Cioppa, and E. Tarantino, in *Proceedings of the IEEE International Conference on Evolutionary Computation*, Perth, Australia, 29 November to 1 December, 1995 (IEEE, New York, 1995), p. 429.

[39]A. Kharal and A. Saleem, Aerosp. Sci. Technol. **23**, 330 (2012).

[40]S. N. Sivanandam and S. N. Deepa, *Introduction to Genetic Algorithms* (Springer-Verlag, Berlin, 2008).

[41]D. Beasley, D. R. Bull, and R. R. Martin, Univ. Comput. **15**, 58 (1993).

[42]S. Lal, K. Yamada, and S. Endo, *Advanced Intelligent Computing Theories and Applications: With Aspects of Artificial Intelligence*, edited by D. S. Huang, D. C. Wunsch II, D. S. Levine, and K. H. Jo (Springer-Verlag, Berlin, 2008), pp. 225–234.

[43]M. Drela, in *Low Reynolds Number Aerodynamics: Proceedings of the Conference, Notre Dame, Indiana, USA, 57 June 1989, Volume 54 of Lecture Notes in Engineering*, edited by T. J. Muleller (Springer-Verlag, New York, 1989), pp. 1–12.